作成上の留意事項

1．「A．研究目的」について
・厚生労働行政の課題との関連性を含めて記入すること。

2．「B．研究方法」について
(1) 実施経過が分かるように具体的に記入すること。
(2) 「（倫理面への配慮）」には、研究対象者に対する人権擁護上の配慮、研究方法による研究対象者に対する不利益、危険性の排除や説明と同意（インフォームド・コンセント）に関わる状況、実験に動物対する動物愛護上の配慮など、当該研究を行った際に実施した倫理面への配慮の内容及び方法について、具体的に記入すること。倫理面の問題がないと判断した場合には、その旨を記入するとともに必ず理由を明記すること。
なお、ヒトゲノム・遺伝子解析研究に関する倫理指針（平成１６年文部科学省・厚生労働省・経済産業省告示第１号）、疫学研究に関する倫理指針（平成１９年文部科学省・厚生労働省告示第１号）、遺伝子治療臨床研究に関する指針（平成１６年文部科学省・厚生労働省告示第２号）、臨床研究に関する倫理指針（平成２０年厚生労働省告示第４１５号）、ヒト幹細胞を用いる臨床研究に関する指針（平成１８年厚生労働省告示第４２５号）、厚生労働省の所管する実施機関における動物実験等の実施に関する基本指針（平成１８年６月１日付厚生労働省大臣官房厚生科学課長通知）及び申請者が所属する研究機関で定めた倫理規定等を遵守するとともに、あらかじめ当該研究機関の長等の承認、届出、確認等が必要な研究については、研究開始前に所定の手続を行うこと。

3．「C．研究結果」について
・当該年度の研究成果が明らかになるように具体的に記入すること。

4．「F．健康危険情報」について
・研究分担者や研究協力者の把握した情報・意見等についても研究代表者がとりまとめて総括研究報告書に記入すること。

5．その他
(1) 日本工業規格A列４番の用紙を用いること。
(2) 文字の大きさは、１０～１２ポイント程度とする。

別紙４

研究成果の刊行に関する一覧表

書籍

著者氏名	論文タイトル名	書籍全体の編集者名	書　籍　名	出版社名	出版地	出版年	ページ

雑誌

発表者氏名	論文タイトル名	発表誌名	巻号	ページ	出版年
Anlifeire A, Hatori M, Morita A, Shiina I, Nakata K, Tosaki Y, Wang Y, Ikekita M, Li G	Ridaifen-G Induces Caspase-independent AtypicalCell Death	Chinese Journal of Cell Biology	33	635- 644	2011

Nagahara Y, Nagamori T, Tamegai H, Hitokuwada M, Yoshimi Y, Ikekita M, Shinomiya T.	Inulin stimulates phagocytosis of PMA-treated THP-1 macrophages by involvement of PI3-kinases and MAP kinases.	Biofactors	37(6)	447-54	2011
Ikeda R, Kurosawa M, Okabayashi T, Takei A, Yoshiwara M, Kumakura T, Sakai N, Funatsu O, Morita A, Ikekita M, Nakaike Y, Konakahara T.	3-(3-Phenoxybenzyl)amino-β-carboline: a novel antitumor drug targeting α-tubulin.	Bioorg Med Chem Lett	21(16)	4784-7	2011
Kuramochi K, Sunoki T, Tsubaki K, Mizushina Y, Sakaguchi K, Sugawara F, Ikekita M, Kobayashi S	Transformation of thiols to disulfides by epolactaene and its derivatives.	Bioorg Med Chem	19(14)	4162-72	2011
Ohashi Y, Iijima H, Yamaotsu N, Yamazaki K, Sato S, Okamura M, Sugimoto K, Dan S, Hirono S, Yamori T.	AMF-26, a Novel Inhibitor of the Golgi System, Targeting ADP-ribosylation Factor 1 (Arf1) with Potential for Cancer Therapy.	J Biol Chem	287(6)	3885-3897	2012
Dan S, Okamura M, Mukai Y, Yoshimi H, Inoue Y, Hanyu A, Sakaue-Sawano A, Imamura T, Miyawaki A, Yamori T.	ZSTK474, a specific phosphatidylinositol 3-kinase inhibitor, induces G1 arrest of the cell cycle in vivo.	Eur J Cancer	48(6)	936-943	2012
Kong D, Yamori T.	JFCR39, a panel of 39 human cancer cell lines, and its application in the discovery and development of anticancer drugs.	Bioorg Med Chem	20(6)	1947-1951	2012
Anzai K, Sekine-Suzuki E, Ueno M, Okamura M, Yoshimi H, Dan S, Yaguchi S, Enami J, Yamori T, Okayasu R.	Effectiveness of combined treatment using X-rays and a phosphoinositide 3-kinase inhibitor, ZSTK474, on proliferation of HeLa cells in vitro and in vivo.	Cancer Sci	102(6)	1176-1180	2011
Hasegawa M, Miura T, Kuzuya K, Inoue A, Ki, SW Horinouchi S, Yoshida T, Kunoh T, Koseki K, Mino K, Sasaki R, Yoshida M, Mizukami T	Identification of SAP155 as the Target of GEX1A (Herboxidiene), An Antitumor Natural Product.	ACS Chem Biol	6	229-233	2011

Ridaifen-G Induces Caspase-independent Atypical Cell Death

Anniwaer Anlifeire[1,2], Manami Hatori[2], Akinori Morita[2], Isamu Shiina[3], Kenya Nakata[3], Yu-Ta Tosaki[3], Yan-Wen Wang[3], Masahiko Ikekita[2], Guan Li[1]*

([1]*College of Life Science, Xinjiang University, Urumqi 830046, China*; [2]*Department of Applied Biological Science, Faculty of Science and Technology, Chiba-ken 278-8510, Japan*; [3]*Department of Applied Chemistry, Faculty of Science, Tokyo University of Science, Tokyo 162-8601, Japan*)

Abstract We have investigated antitumor activities of Ridaifens (RIDs), which are a series of synthesized Tamoxifen (TAM) derivatives. In this study, we focused on one of RIDs, Ridaifen-G (RID-G), and investigated the cell death-inducing activity of it in four neoplastic hematopoietic cell lines, U937, Raji, THP-1, and IM-9 cells in the presence or absence of a pan-caspase inhibitor, Z-VAD-fmk. The aim of this study is to characterize the mode of RID-G-induced cell death, as compared with a typical apoptosis of etoposide-treated U937 cells, which die mainly through mitochondria-mediated apoptotic pathway in a caspase-dependent manner. To obtain reliable results, we analyzed RID-G-induced cell death by four methods, i.e., MTT assay, MitoTracker staining, AnnexinV-FITC/Propidium Iodide double staining, and DNA ladder formation. These analyses revealed that RID-G-induced cell death is accompanied by mitochondrial dysfunction and executed in a caspase-independent manner except DNA ladder formation. Z-VAD-fmk did not suppress the death, but suppressed etoposide-induced apoptosis in U937 cells. In DNA ladder formation analysis, RID-G induced a smear of DNA fragmentation in Raji and THP-1 cells, and RID-G-treated U937 cells showed less DNA ladder formation than when treated with etoposide. In addition, Z-VAD-fmk showed different effects on these DNA fragmentations: it largely suppressed, partialy suppressed, and on the contrary, enhanced DNA fragmentaion in U937, THP-1, and Raji cells, respectively. These results suggest that RID-G induces caspase-independent atypical cell death, which is accompanied by mitochondrial dysfunction.

Key words cell death; mitochondria; caspase; apoptosis; Ridaifen-G

Apoptosis, or programmed cell death, is a normal component of the development and health of multicellular organisms. Cells die in response to a variety of stimuli and during apoptosis they do so in a controlled, regulated fashion. This makes apoptosis distinct from another form of cell death called necrosis in which uncontrolled cell death leads to lysis of cells, inflammatory responses and, potentially, to serious health problems. Apoptosis, by contrast, is a process in which cells play an active role in their own death (which is why apoptosis is often referred to as cell suicide).

Mitochondria play an important role in the regulation of apoptosis(Fig.1). With multiple cytotoxic stimuli, including UV, X-ray, and many chemical drugs, mitochondrial perturbation occurs by mitochondrial membrane potential ($\Delta\Psi_m$) reduction and cytochrome *c* (Cyt *c*) release into the cytosol[1,2]. Bcl-2 family proteins are involved in the stability of the mitochondrial membrane by promoting or preventing mitochondrial perturbation[3~5]. When mitochondrial stability is attenuated, released Cyt *c* binds to the cytosolic adaptor protein, apoptotic protease activating factor-1 (Apaf-1), and the complex activates one of the initiator caspases, caspase-9[6]. Activated caspase-9 in turn activates the effector caspases (caspase-3, -6, and -7) to implement apoptosis by means of chromatin DNA fragmentation, morphological changes, and cell-volume loss. Overall,

Received: January 19, 2011 Accepted: March 3, 2011

*Corresponding author. Tel: 86-991-8581106, E-mail: guanli@xju.edu.cn

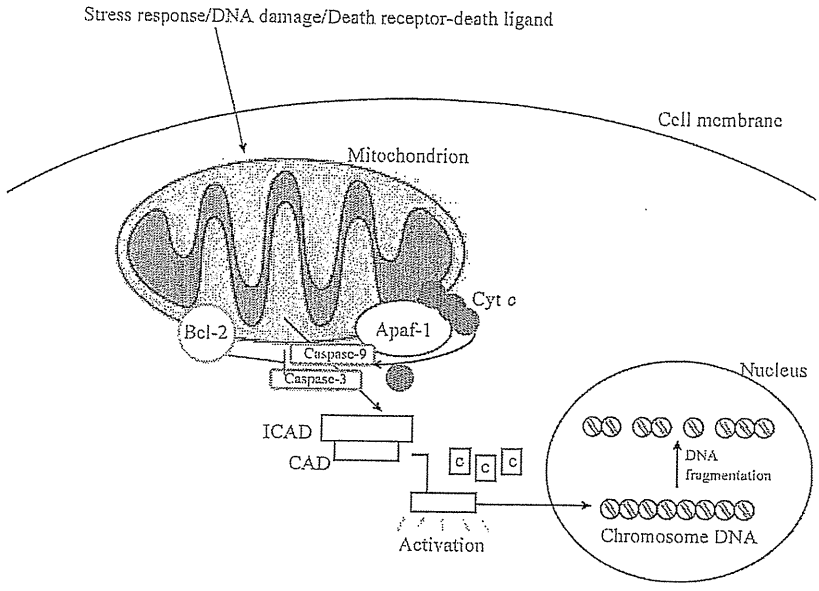

Fig.1 Role of mitochondria in apoptosis

mitochondrial perturbation tends to induce apoptosis. However, mitochondria participated in TAM-induced apoptosis is not clear. Mandlekar[7] discovered that caspase-9 is slightly activated during TAM-induced apoptosis, suggesting mitochondrial participation. In contrast, Ferlini[8] has reported that mitochondria-localized anti-apoptotic protein Bcl-2 expression and functional inactivation by phosphorylation is unchanged during TAM-induced apoptosis, assuming that TAM-induced apoptosis is independent of mitochondria.

We have recently developed a rapid synthesis of pseudo-symmetrical TAM derivatives, Ridaifens (RIDs)[9~13]. RIDs can be synthesized as novel analogues of TAM, and one of RIDs, Ridaifen-B (RID-B) shows more potent apoptosis-inducing activity than the original TAM[9]. In the present study, we focused on a conformational analog of RID-B, RID-G, and investigated the cell death-inducing activity of it in several neoplastic hematopoietic cell lines. Our cell death analyses by four methods in the presence or absence of a pan-caspase inhibitor, Z-VAD-fmk, revealed that RID-G-induced cell death is accompanied by mitochondrial dysfunction in a caspase-independent manner.

1 Materials and Methods

1.1 Cell culture and treatment

The human monoblastic lymphoma cell line U937, the human multiple myeloma cell line IM-9, the human Burkitt's lymphoma cell line Raji, and the human acute monocytic leukemia cell line THP-1 were cultured in RPMI 1640 medium (Wako, Japan) supplemented with 10% fetal bovine serum (FBS, Gibco, USA). Cells were maintained at 37 °C in a humidified atmosphere containing 5% CO_2. Cells were counted with a cell counter (Z1 Cell and particle counter, Beckman Coulter, USA). RID-G was chemically synthesized in our laboratory at Tokyo University of Science (Fig.2)[10~13]. Etoposide and Z-VAD-FMK were purchased from Wako and Peptide Institute (Japan), respectively. These agents were dissolved in dimethyl sulfoxide at stock concentrations of 10 mmol/L. Cells were seeded into plates or flasks (Becton Dickinson, USA) at concentrations of 2×10^5 cells/ml unless otherwise specified, and preincubated at 37 °C for 18 h. The cells were then treated with 5 μmol/L RID-G, and U937 cells were also treated with 5 μmol/L etoposide for indicated periods in the presence or absence of 20 μmol/L Z-VAD-fmk. Z-VAD-fmk was added to the

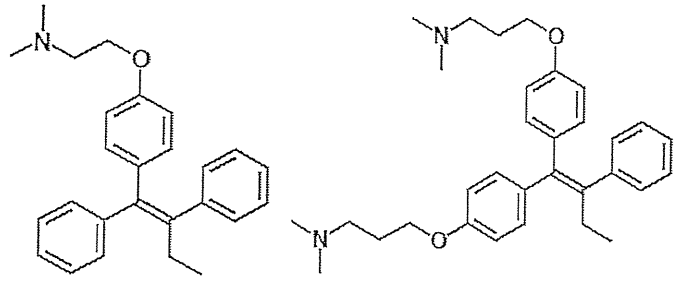

Tamoxifen Ridaifen-G (RID-G)

Fig.2 Chemical structures of tamoxifen and its derivative RID-G

culture medium immediately before RID-G or etoposide treatment.

1.2 MTT assay

After the chemical treatments described above, cell viability was determined by MTT assay[14,15], a method for determining cell viability by measuring the mitochondrial dehydrogenase activity. In this assay, 11 μl of MTT stock solution (5 mg/ml in phosphate-buffered saline (PBS)) was added to each well in a 96-well plate (Becton Dickinson), and the plate was incubated at 37 °C for 1 h. After centrifugation for 5 min at 1 500 r/min, the supernatant was discarded, and 100 μl of DMSO was added to each well to dissolve MTT formazan. Absorbance at 570 nm was measured with a microplate reader (Model 550, Bio-Rad, USA), and the cell viabilities were defined as the percentage of the absorbance values compared with the absorbance value of vehicle-treated control[15].

1.3 Flow cytometric analysis

For each sample, 10 000 cells were analyzed with a flow cytometer (FACS Calibur, Becton Dickinson)[16]. The percentage of cell death was determined by Annexin V-FITC and Propidium Iodide (PI) double staining using a MEBCYTO Apoptosis Kit (MBL, Japan) according to the manufacturer's instructions. Early stage cell death was defined as the percentage of Annexin V-positive and PI-negative cells, and late stage cell death was defined as the percentage of Annexin V/PI-double positive cells. The percentage of cells losing their $\Delta\Psi_m$ was determined by MitoTracker staining. After the treatments, cells were incubated in culture medium for 30 min at 37 °C with 100 nmol/L MitoTracker Red CMXRos dye (Invitorgen, USA). The cells were then washed twice, suspended in ice-cold PBS, and analyzed by flow cytometer.

1.4 DNA fragmentation analysis

The chemical treatments in this analysis were performed at cell densities of 8×10^5 cells/ml. For DNA extraction, 1×10^6 cells were suspended in 200 μl of PBS, and lysed by adding 50 μl of lysis buffer (50 mmol/L EDTA-NaOH, pH8.0, 3% Sarkosyl), and 50 μl of RNase A (10 mg/ml) for 2 h at 56 °C followed by 30 μl of proteinase K (10 mg/ml in PBS) overnight incubation at 56 °C. Cellular genomic DNAs were then extracted from the lysates by phenol-chloroform extractions, and 70% ethanol precipitation. Aliquots of 2 μg of cellular DNA were separated by electrophoresis on a 1.5% agarose gel, and stained with 1 μg/ml ethidium bromide and visualized under UV light.

2 Results

2.1 RID-G-induced cell death is accompanied by mitochondrial dysfunction

In the process of apoptosis, mitochondrial disruption occurs, resulting in the decrease of mitochondrial dehydrogenase activity and the loss of $\Delta\Psi_m$. To detect whether these events are induced by RID-G, we analyzed the effects of RID-G on four neoplastic hematopoietic cell lines by MTT assay and MitoTracker staining. As shown in Figure 3 and Figure 4, these

analyses showed that RID-G induced mitochondrial dysfunction. In MTT assay (Fig.3), approximately 85% decrease in cell viability was detected in U937, THP-1, and Raji cells by RID-G or etoposide treatment, and IM-9 cells showed a relative resistance to RID-G (50% decrease). In addition, IC_{50} values of U937, IM-9, THP-1, and Raji cells in MTT assay at 8 h after RID-G treatment were 3.2 μmol/L, 7.0 μmol/L, 2.6 μmol/L, and 2.3 μmol/L, respectively (data not shown). Therefore, we used U937, THP-1, and Raji cells as RID-G-sensitive cell lines, and IM-9 cells were used as a relatively resistant cell line.

In MitoTracker staining analysis (Fig.4), these cell lines showed similar sensitivities to RID-G as that observed in MTT assay, since U937, THP-1, and Raji cells were highly sensitive (approximately

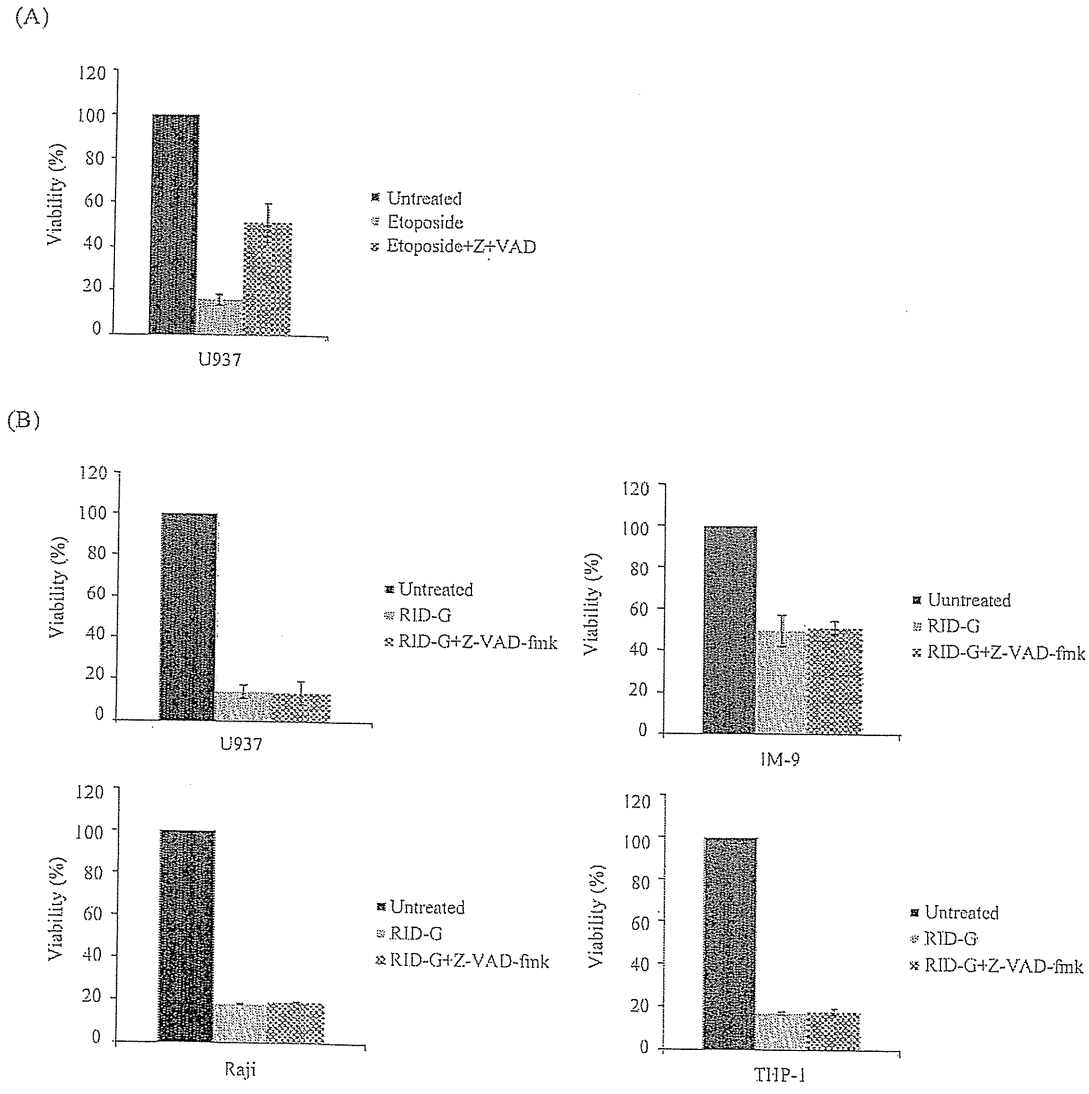

Fig.3 Effects of Z-VAD-fmk on RID-G or etoposide-induced cell death determined by MTT assay

RID-G, etoposide, and Z-VAD-fmk were used at final concentrations of 5 μmol/L, 5 μmol/L, and 20 μmol/L, respectively. The cell viabilities quantified by MTT assay were determined at 4 h (RID-G) or 18 h (etoposide) after treatment. Data shown were means±SD from 3 independent experiments. A: Z-VAD-fmk suppresses etoposide-induced cell death in U937 cells; B: Z-VAD-fmk can not suppress RID-G-induced cell death in U937, IM-9, THP-1, and Raji cells.

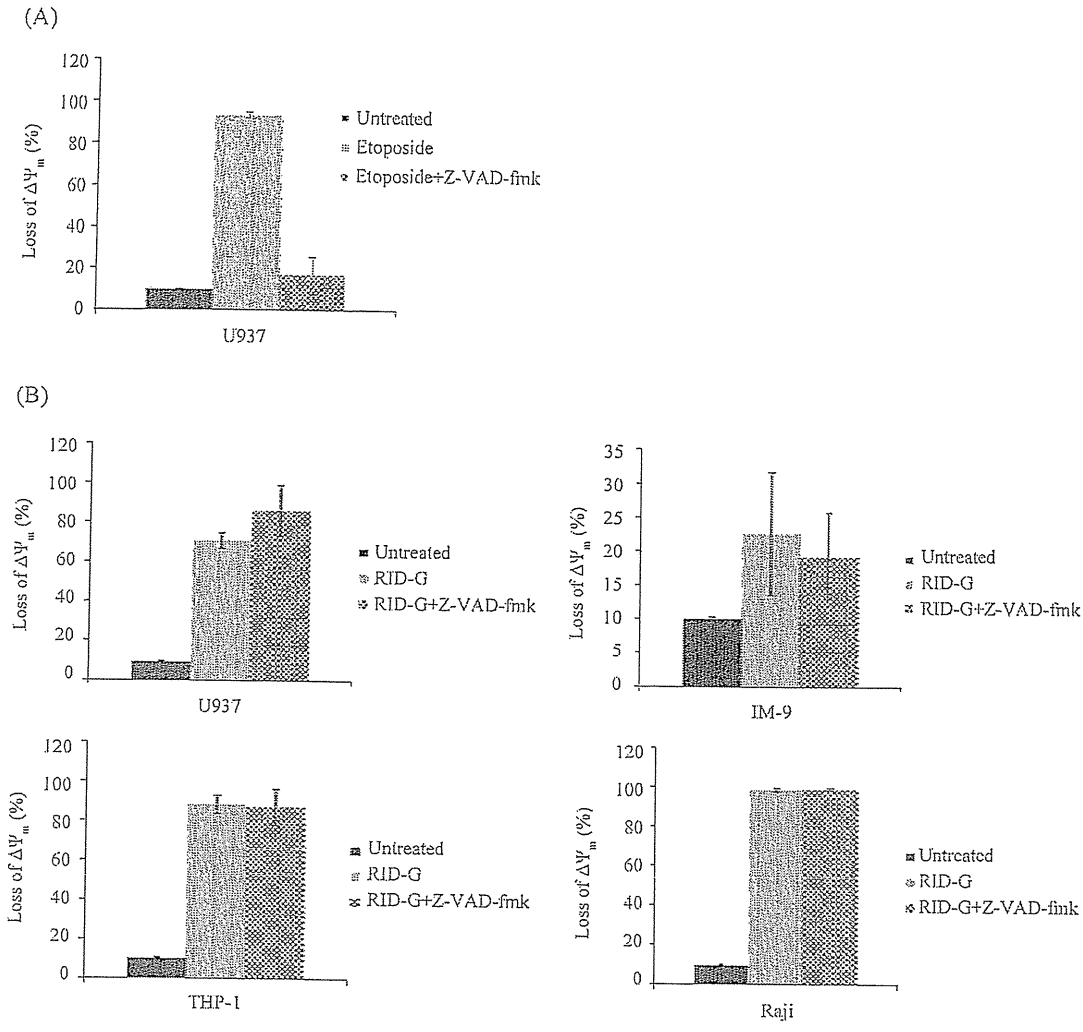

Fig.4 Effects of Z-VAD-fmk on RID-G or etoposide-induced loss of mitochondrial membrane potential ($\Delta\Psi_m$) determined by MitoTracker staining

RID-G, etoposide, and Z-VAD-fmk were used at final concentrations of 5 μmol/L, 5 μmol/L, and 20 μmol/L, respectively. The loss of $\Delta\Psi_m$ quantified by flow cytometric analysis after MitoTracker staining was measured at 6 h (RID-G) or 18 h (etoposide) after treatment. Data shown were means±SD from 3 independent experiments. A: Z-VAD-fmk suppresses etoposide-induced loss of $\Delta\Psi_m$ in U937 cells; B: Z-VAD-fmk can not suppress RID-G-induced loss of $\Delta\Psi_m$ in U937, IM-9, THP-1, and Raji cells.

70%~99% of cells lose their $\Delta\Psi_m$), and IM-9 cells were resistant to RID-G (only a 23% rise). Furthermore, these RID-G-induced mitochondrial changes were not suppressed by a pan-caspase inhibitor, Z-VAD-fmk (Fig.3B and Fig.4B), although Z-VAD-fmk suppressed etoposide-induced mitochondrial changes in U937 cells (Fig.3A and Fig.4A). These data indicate that RID-G, unlike etoposide, induces a caspase-independent mitochondrial dysfunction.

2.2 RID-G induces an early apoptotic change

To pursue the caspase-independent mechanism, we also analyzed the cells by Annexin V-FITC/PI double staining (Fig.5). The flow cytometric analysis detects the early apoptotic changes i.e., the cell-surface exposure of phosphatidylserine by FITC-labeled Annexin V. In conjunction with a dye exclusion

of PI, this analysis also discriminates intact cells ($FITC^-/PI^-$), early apoptotic cells ($FITC^+/PI^-$), and late apoptotic or necrotic cells ($FITC^+/PI^+$)[17]. In this analysis, RID-G predominantly induced a $FITC^+/PI^-$ early apoptotic change in all cell lines, suggesting that RID-G fundamentally elicit apoptotic signals, but not necrotic signals. Interestingly, the sensitivity of IM-9 cells to RID-G is comparable to the sensitivities of other cells in spite of their resistance to mitochondrial dysfunction. Again, Z-VAD-fmk failed to suppress RID-G-induced cell death (Fig.5B), although Z-VAD-fmk suppressed the etoposide-induced apoptosis in U937 cells (Fig.5A). These data further support our observations that the mode of action of RID-G is caspase-independent. We therefore speculate that RID-G induces a caspase-independent apoptosis in

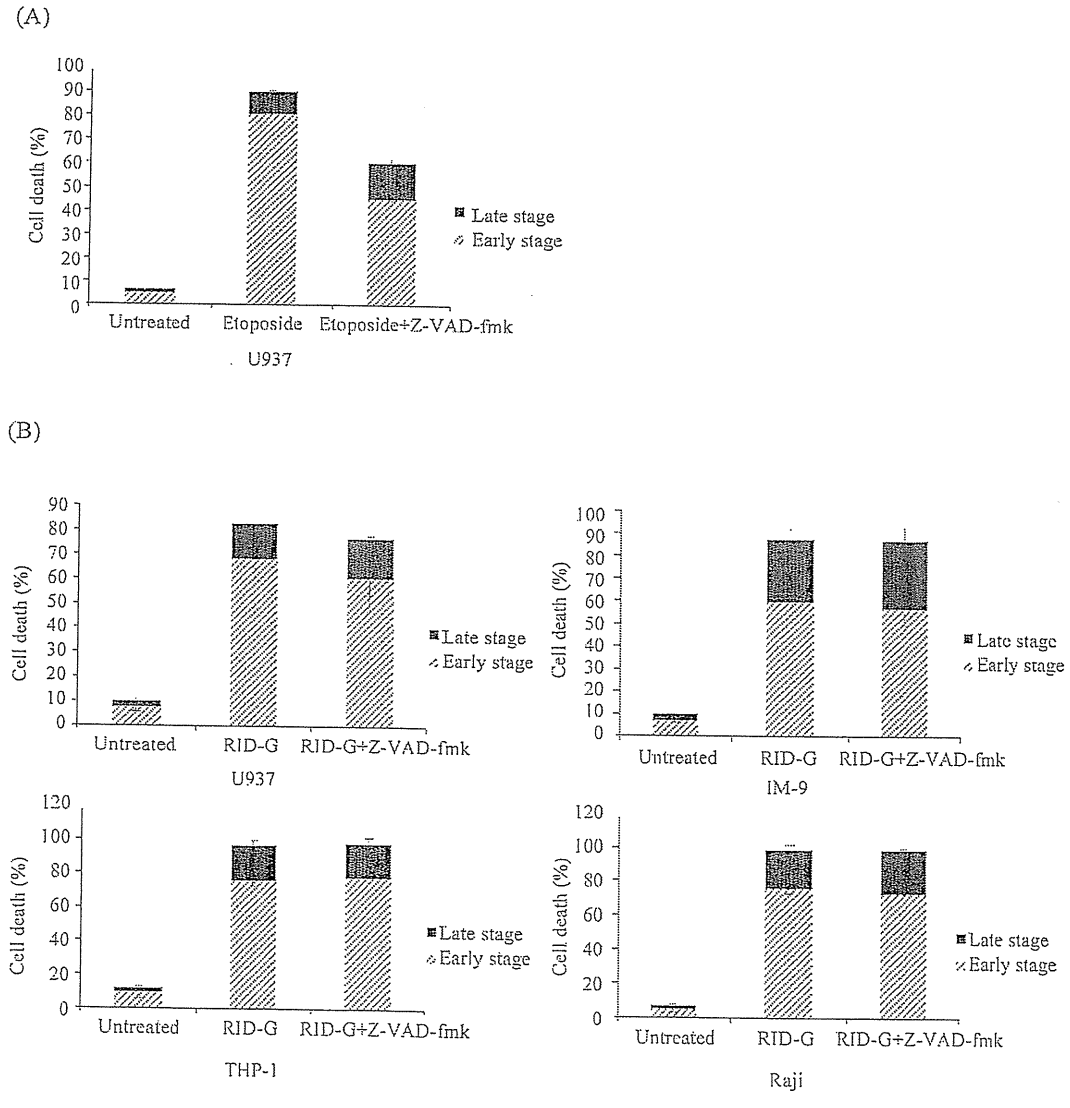

Fig.5 Effects of Z-VAD-fmk on RID-G or etoposide-induced cell death determined by Annexin V-FITC/PI double staining methods

RID-G, etoposide, and Z-VAD-fmk were used at final concentrations of 5 μmol/L, 5 μmol/L, and 20 μmol/L, respectively. The percentages of early and late cell death stages were determined at 6 h (RID-G) or 18 h (etoposide) after treatment. Early stage and late stage indicate $FITC^+/PI^-$ and $FITC^+/PI^-$ cells, respectively. Data shown were means±SD from 3 independent experiments. A: Z-VAD-fmk suppresses etoposide-induced cell death in U937 cells; B: Z-VAD-fmk cannot suppress RID-G-induced cell death in U937, IM-9, THP-1, and Raji cells.

these cells.

2.3 RID-G induces DNA fragmentation, but its pattern varies among cell lines

To further characterize RID-G-induced cell death is apoptosis or the other mode of cell death, we performed DNA fragmentation analysis in order to confirm whether the pattern of DNA fragmentation is the typical apoptotic "DNA ladder" or not. As shown in Figure 6, RID-G induced a DNA ladder formation in U937 cells, but the cells showed less DNA ladder formation than when treated with etoposide, and, surprisingly, RID-G induced smear of DNA fragmentations in Raji and THP-1 cells, suggesting that the cell death is not typical apoptosis. On the other hand, IM-9 cells did not show any DNA fragmentation 6 h after RID-G treatment, possibly by their resistance to mitochondrial dysfunction (data not shown). Furthermore, Z-VAD-fmk showed inconsistent effects on these DNA fragmentations: it largely suppressed, partialy suppressed, and on the contrary, enhanced DNA fragmentaion in U937, THP-1, and Raji cells, respectively. These results suggest that the machinery for typical caspase-dependent apoptotic DNA fragmentation is partially activated in RID-G-treated U937 cells, and that typical DNA degradations occur in a caspase-dependent and a caspase-suppressible manner in THP-1 and Raji cells, respectively.

Taken together, Table 1 shows a summary of effects of Z-VAD-fmk on RID-G or etoposide-induced cell death in U937 cells. These data indicate that RID-G mainly induces caspase-independent cell death accompanied with mitochondrial dysfunction, and the

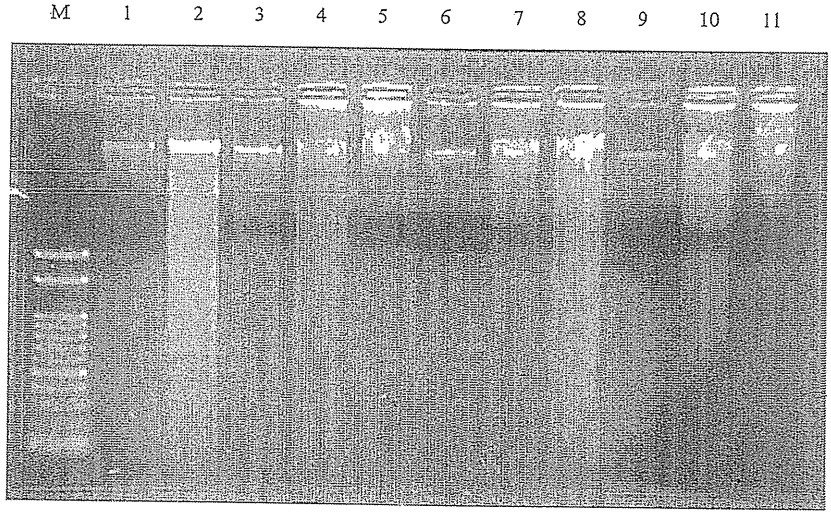

Fig.6 Effects of Z-VAD-fmk on RID-G or etoposide-induced cell death detected by DNA ladder formation

RID-G, etoposide, and Z-VAD-fmk were used at final concentrations of 5 μmol/L, 5 μmol/L, and 20 μmol/L, respectively. The DNA ladder formation was detected by agarose gel electrophoresis. Cells were harvested at 6 h (RID-G) or 18 h (etoposide) after treatment. M: 100 bp ladder marker; lane 1: untreated U937; lane 2: etoposide-treated U937; lane 3: etoposide + Z-VAD-fmk-treated U937; lane 4: RID-G-treated U937; lane 5: RID-G + Z-VAD-fmk-treated U937; lane 6: untreated Raji; lane 7: RID-G-treated Raji; lane 8: RID-G + Z-VAD-fmk-treated Raji; lane 9: untreated THP-1; lane 10: RID-G-treated THP-1; lane 11: RID-G + Z-VAD-fmk-treated THP-1.

Table 1 Summary of effects of Z-VAD-fmk on RID-G or etoposide-induced cell death in U937 cells

Groups	RID-G	RID-G+Z-VAD-fmk	Etoposide	Etoposide+Z-VAD-fmk
MTT assay	+	+	+	-
MitoTracker	+	+	+	-
Annexin V-FITC/PI	+	+	+	-
DNA ladder	+	-	++	-

+: cell death is induced; ++: cell death is more strongly induced than RID-G treatment; -: cell death is suppressed.

late apoptotic event such as DNA fragmentation is mediated by caspases in some cell lines.

3 Discussion

In the present study, we showed that RID-G mainly induces caspase-independent cell death accompanied by mitochondrial dysfunction in four neoplastic hematopoietic cell lines, U937, Raji, THP-1, and IM-9 cells, and that the patterns of RID-G-induced DNA fragmentations are different among cell lines through the mechanisms that can not be explained by the classical caspase-dependent mechanism alone.

Mitochondrion is the key factor involved in apoptosis; the current view is that the mitochondrion is not only an initiator of apoptosis, but also an amplifier of apoptotic signals. The important feature of apoptosis is a permeability change in the mitochondrial membrane, which is the central link in the general apoptotic pathway. The mitochondrial outer membrane permeabilization leads to the release of a variety of apoptogenic proteins such as Cyt *c*[2,18,19], second mitochondria-derived activator of caspase/direct IAP-binding protein with low PI (Smac/Diablo)[20~23], Omi/HtrA2[24,25], apoptosis inducing factor (AIF)[26], and endonuclease G (EndoG)[27] from mitochondria into cytosol, resulting in the mitochondrial dysfunction including the loss of $\Delta\Psi_m$ and the uncoupling of the respiratory chain.

During these mitochondrial changes, caspases play a role in enhancing the mitochondrial disruption through cleavages of some Bcl-2 family proteins such as Bcl-2, Bcl-xL, and Bid. The irreversible cleavages can switch them from anti- to pro-apoptotic property in Bcl-2 and Bcl-xL[28~30], and convert Bid from mildly to strongly apoptotic[5,31], which are considered as a possible cause of the effectiveness of Z-VAD-fmk in suppressing etoposide-induced mitochondrial dysfunction in U937 cells (Fig.3A and Fig.4A). On the other hand, Z-VAD-fmk did not show any inhibitory activity against RID-G-induced mitochondrial dysfunction (Fig.3B and Fig.4B). The results indicate that the caspase-mediated enhancement is dispensable for RID-G-induced mitochondrial dysfunction, which could be explained solely by an initial damage by RID-G alone due to its strong ability to impair mitochondria. This would also raise the possibility that the damage is too excessive to prevent death such as necrosis. However, RID-G-induced death is probably not necrosis, because the death exhibited an early apoptotic change in the flow cytometric analysis using Annexin V-FITC/PI double staining (Fig.5). Explorations of the target molecules of RID-G may provide new insight into the intracellular mechanisms of cell death.

In DNA fragmentation analysis, the pattern of RID-G-induced DNA fragmentation and the response of the fragmentation to Z-VAD-fmk varied among cell lines (Fig.6). The fact that these RID-G-treated cells died regardless of the presence or absence of Z-VAD-fmk as assessed by three different methods (Fig.3~Fig.5) indicates that the suppressions of DNA fragmentation by Z-VAD-fmk in U937 and THP-1 cells does not mean the recovery from the death, but merely mean the mechanistic inhibition of the final step(s) of the cell death. The fragmentation of DNA into nucleosomal units is caused by an enzyme known as caspase activated DNase (CAD). Normally, CAD exists as an inactive complex with ICAD (inhibitor of CAD). During apoptosis, ICAD is cleaved by caspases such as caspase-3, to release CAD, followed by rapid internucleosomal fragmentation of the nuclear DNA[32,33]. The culprit of the DNA fragmentation could be CAD and/or CAD-like nuclease, because the fragmentation is a typical "DNA ladder" and inhibited by Z-VAD-fmk, which indicates that the responsible nuclease is a caspase-dependent one that cause internucleosomal DNA fragmentation. In contrast, the responsible nuclease(s) in THP-1 and Raji cells are considered not to be CAD, since the fragmentation in these cells is a smear of DNA fragmentation. Considering the strong activity of RID-G against mitochondria, the nucleases in THP-1 and Raji cells may be other nuclear DNA degrading factors released from the mitochondria, e.g., EndoG and AIF, although

how caspases involved in these DNA fragmentations in THP-1 and Raji cells is unclear. Especially, EndoG is reported to induce a smear of DNA fragmentation[34]. This hypothesis further supported by our observation that the RID-G-resistant cell line, IM-9 cells, showed a resistance to DNA fragmentation (data not shown) as well as mitochondrial dysfunction (Fig.3 and Fig.4).

Taken together, RID-G has a strong cell death-inducing activity, and may induce a novel mode of cell death. RID-G may serve to develop a new type of anticancer drugs. The modes of cell death are recently classified into several modes including apoptosis, necrosis, autophagy, mitotic catastrophe, and so on[35,36]. Further investigations are warranted to determine whether RID-G-induced cell death can be classified into one of those classifications or not.

References

1 Zamzami N, Marzo I, Susin SA, Brenner C, Larochette N, Marchetti P, *et al.* The thiol crosslinking agent diamide overcomes the apoptosis-inhibitory effect of Bcl-2 by enforcing mitochondrial permeability transition. Oncogene 1998; 16(8): 1055-63.

2 Liu XS, Kim CN, Yang J, Jemmerson R, Wang XD. Induction of apoptotic program in cell-free extracts: requirement for dATP and cytochrome *c*. Cell 1996; 86(1): 147-57.

3 Narita M, Shimizu S, Ito T, Chittenden T, Lutz RJ, Matsuda H, *et al.* Bax interacts with the permeability transition pore to induce permeability transition and cytochrome *c* release inisolated mitochondria. Proc Natl Acad Sci USA 1998; 95(25): 14681-6.

4 Zha J, Harada H, Osipov K, Jockel J, Waksman G, Korsmeyer SJ. BH_3 domain of BAD is required for heterodimerization with Bcl-xL and proapoptotic activity. J Biol Chem 1997; 272(39): 24101-4.

5 Luo X, Budihardjo I, Zou H, Slaughter C, Wang X. Bid, a Bcl2 interacting protein, mediates cytochrome *c* release from mitochondria in response toactivation of cell surface death receptors. Cell 1998; 94(4): 481-90.

6 Li P, Nijhawan D, Budihardjo I, Srinivasula SM, Ahmad M, Alnemri ES, *et al.* Cytochrome *c* and dATP-dependent formation of Apaf-1/caspase-9 complex initiates an apoptotic protease cascade. Cell 1997; 91(4): 479-89.

7 Mandlekar S, Yu R, Tan TH, Kong AN. Activation of caspase-3 and c-JunNH_2-terminal kinase-1 signaling pathways in tamoxifen-induced apoptosis of human breast cancer cells. Cancer Res 2000; 60(21): 5995-6000.

8 Ferlini C, Scambia G, Marone M, Distefano M, Gaggini C, Ferrandina G, *et al.* Tamoxifen induces oxidative stress and apoptosis in oestrogen receptor-negative human cancer cell lines. Br J Cancer 1999; 79(2): 257-63.

9 Nagahara Y, Shinna I, Nakata K, Sasaki A, Miyamoto T, Ikekita M. Induction of mitochondria-involved apoptosis in estrogen receptor-negative cells by a novel tamoxifen derivative, ridaifen-B. Cancer Sci 2008; 99(3): 608-14.

10 Shiina I, Suzuki M, Yokoyama K. Short-step synthesis of tamoxifen and its derivatives via the three-component coupling reaction and migration of the double bond. Tetrahedron Lett 2004; 45(5): 965-7.

11 Shiina I, Sano Y, Nakata K, Kikuchi T, Sasaki A, Ikekita M, *et al.* Synthesis of the new pseudo-symmetrical tamoxifen derivatives and their anti-tumor activity. Bioorg Med Chem Lett 2007; 38(36): 2421-4.

12 Shiina I, Sano Y, Nakata K, Suzuki M, Yokoyama T, Sasaki A, *et al.* An expeditious synthesis of tamoxifen, a representative SERM (selective estrogen receptor modulator), via the three-component coupling reaction among aromatic aldehyde, cinnamyltrimethylsilane, and β-chlorophenetole. Bioorg Med Chem 2007; 15(24): 7599-617.

13 Shiina I, Sano Y, Nakata K, Kikuchi T, Sasaki A, Ikekita M, *et al.* Synthesis and pharmacological evaluation of the novel pseudo-symmetrical tamoxifen derivatives as anti-tumor agents. Biochem Pharm 2008; 75(5): 1014-26.

14 Alley MC, Scudiero DA, Monks A, Hursey ML, Czerwinski MJ, Fine DL, *et al.* Feasibility of drug screening with panels of human tumor cell lines using a microculture tetrazolium assay. Cancer Res 1988; 48(3): 589-601.

15 Nakai J, Kawada K, Nagata S, Kuramochi K, Uchiro H, Kobayashi S, *et al.* A novel lipid compound, epolactaene, induces apoptosis: Its action is modulated by its side chain structure. Biochim Biophys Acta 2002; 1581(1-2): 1-10.

16 Morita A, Zhu J, Suzuki N, Enomoto A, Matsumoto Y, Tomita M, *et al.* Sodium orthovanadate supprese DNA damage-induced caspase activation and apoptosis by inactivating p53. Cell Death Differ 2006; 13(3): 499-511.

17 Vermes I, Haanen C, Steffens-Nakken H, Reutelingsperger C. A novel assay for apoptosis. Flow cytometric detection of phosphatidylserine expression on early apoptotic cells using fluorescein labelled annexin V. J Immunol Methods 1995; 184(1): 39-51.

18 Kluck RM, Wetzel EB, Green DR, Newmwyer DD. The release of cytochrome *c* from mitochondria: A primary site for Bcl-2 regulation of apoptosis. Science 1997; 275(5303): 1132-6.

19 Yang J, Liu XS, Bhalla K, Kim CN, Ibrabo AM, Cai JY, *et al.* Prevention of apoptosis by Bcl-2: Release of cytochrome *c* from mitochondria blocked. Science 1997; 275(5303): 1129-32.

20 Du CY, Fang M, Li YC, Li LY, Wang XD. Smac, a mitochondrial protein that promotes cytochrome *c*-dependent caspase activation by elimination IAP inhibition. Cell 2000; 102(1): 33-42.

21 Verhagen AM, Ekert PG, Pakusch M, Silke J, Connolly LM, Reid GE, *et al.* Identification of DIABLO, a mammalian protein that

promotes apoptosis by binding to and antagonizing IAP proteins. Cell 2000; 102(1): 43-53.
22 Liu Z, Sun C, Olejinicazak ET, Meadows RP, Betz SF, Oost T, *et al.* Structural basis for binding of Smac/DIABLO to the XIAP BIR3 domain. Nature 2000; 408(6815): 1004-8.
23 Wu G, Chai JJ, Suber TL, Wu JW, Du CY, Wang XD, *et al.* Structural basis of IAP recognition by Smac/DIABLO. Nature 2000; 408(6815): 1008-12.
24 Hegde R, Srinivasula SM, Zhang ZJ, Wassell R, Mukattash R, Cilenti L, *et al.* Identification of Omi/HtrA2 as a mitochondrial apoptotic serine protease ehat disrupts inhibitor of apoptosis protein-caspase interaction. J Biol Chem 2002; 277(1): 432-8.
25 Martins LM, Iaccarino I, Tenev T, Gschmeissner S, Totty NF, Lemoine NR, *et al.* The serine protease Omi/HtrA2 regulates apoptosis binding XIAP through a reaper-like motif. J Biol Chem 2002; 277(1): 439-44.
26 Susin SA, Lorezo HK, Zamzami N, Marzo I, Snow BE, Brothers GM, *et al.* Molecular characterization of mitochondrial apoptosis-inducing factor. Nature 1999; 397(6718): 441-6.
27 Li LY, Luo X, Wang XD. Endonuclease G is an apoptotic DNase when released from mitochondria. Nature 2001; 412(6842): 95-9.
28 Cheng EH, Kirsch DG, Clem RJ, Ravi R, Kastan MB, Bedi A, *et al.* Conversion of Bcl-2 to a Bax-like death effector by caspase. Science 1997; 278(5345): 1966-8.
29 Clem RJ, Cheng EH, Karp CL, Kirsch DG, Ueno K, Takahashi A, *et al.* Modulation of cell death by Bcl-xL through caspase interaction. Proc Natl Acad Sci USA 1998; 95(2): 554-9.
30 Bellows DS, Chau BN, Lee P, Lazebnik Y, Burns WH, Hardwick JM. Antiapoptotic herpesvirus Bcl-2 homologs escape caspase-mediated conversion to proapoptotic proteins. J Virol 2000; 74(11): 5024-31.
31 Li H, Zhu H, Xu CJ, Yuan J. Cleavage of BID by caspase 8 mediates the mitochondrial damage in the Fas pathway of apoptosis. Cell 1998; 94(4): 491-501.
32 Enari M, Sakahira H, Yokoyama H, Okawa K, Iwamatsu A, Nagata S. A caspase-activated DNase that degrades DNA during apoptosis, and its inhibitor ICAD. Nature 1998; 391(6662): 43-50.
33 Sakahira H, Enari M, Nagata S. Cleavage of CAD inhibitor in CAD activation and DNA degradation during apoptosis. Nature 1998; 391(6662): 96-9.
34 Loo GV, Schotte P, Gurp MV, Demol H, Hoorelbeke B, Gevaert K, *et al.* Endonuclease G: A mitochondrial protein released in apoptosis and involved in caspase-independent DNA degradation. Cell Death Differ 2001; 8(12): 1136-42.
35 Kroemer G, Galluzzi L, Vandenabeele P, Abrams J, Alnemri ES, Baehrecke EH, *et al.* Classification of cell death: Recommendations of the nomenclature committee on cell death 2009. Cell Death Differ 2009; 16(1): 3-11.
36 Galluzzi L, Maiuri MC, Vitale I, Zischka H, Castedo M, Zitvogel L, *et al.* Cell death modalities: Classification and pathophysiological implications. Cell Death Differ 2007; 14(7): 1237-43.

Ridaifen-G诱导细胞死亡不依赖于细胞凋亡蛋白酶

安里菲热·安尼瓦尔[1,2] 羽鸟麻奈美[2] 森田明典[2] 椎名勇[3]
中田健也[3] 户崎雄太[3] 王艳雯[3] 池北雅彦[2] 李 冠[1*]
([1]新疆大学生命科学与技术学院, 乌鲁木齐 830046; [2]东京理科大学理工学部应用生物科学科, 千叶县 278-8510;
[3]东京理科大学理学部应用化学科, 东京 162-8601)

摘要 通过对Ridaifen-G(RID-G)诱导造血细胞U937、Raji、THP-1和IM-9死亡是否需要Z-VAD-fmk(一种细胞凋亡蛋白酶抑制剂)的研究, 发现RID-G以细胞凋亡蛋白酶非依存性的方式诱导细胞死亡, 并伴随有线粒体功能紊乱。Z-VAD-fmk对U937细胞的死亡没有影响, 但抑制etoposide诱导的细胞凋亡; DNA片段化结果表明, RID-G可破坏Raji和THP-1细胞的DNA, 经RID-G处理后的U937细胞的DNA条带没有经etoposide处理的清晰。此外, Z-VAD-fmk对U937、THP-1和Raji细胞DNA的片段化程度有不同的影响, 抑制细胞死亡。这些结果表明, RID-G诱导的非典型细胞死亡不依赖于caspase, 且伴随有线粒体功能紊乱。

关键词 细胞死亡; 线粒体; 细胞凋亡蛋白酶; 细胞凋亡; Ridaifen-G

收稿日期: 2011-01-19 接受日期: 2011-03-03
*通讯作者。Tel: 0991-8581106, E-mail: guanli@xju.edu.cn

Research Communication

BioFactors

Inulin stimulates phagocytosis of PMA-treated THP-1 macrophages by involvement of PI3-kinases and MAP kinases

Yukitoshi Nagahara,[1] Taome Nagamori,[1] Hidekazu Tamegai,[1] Mami Hitokuwada,[1] Yoji Yoshimi,[2] Masahiko Ikekita,[2] and Takahisa Shinomiya[1,2]*

[1]*Department of Biotechnology, College of Science and Engineering, Tokyo Denki University, Hatoyama, Hiki-gun, Saitama, Japan*

[2]*Department of Applied Biological Science, Faculty of Science and Technology, Tokyo University of Science, Noda, Chiba, Japan*

Abstract.

Inulin is a polysaccharide that enhances various immune responses, mainly to T and B cells, natural killer cells, and macrophages *in vivo* and *in vitro*. Previous reports describe that inulin activates macrophages indirectly by affecting the alternative complement pathway. In this study, we examined the direct effect of inulin on PMA-treated THP-1 macrophages. Inulin treatment did not stimulate the proliferation of THP-1 macrophages at all. However, inulin treatment significantly increased phagocytosis of the polystyrene beads without the influence of serum. Doses of around 1 mg/mL had the maximal effect, and significant progression of phagocytosis occurred at times treated over 6 h. Inulin augmented phagocytosis not only with polystyrene beads but also with apoptotic cancer cells. The inulin-induced phagocytosis uptake was suppressed in Toll-like receptor (TLR) 4 mutated C3H/HeJ mice peritoneal macrophages. Moreover, inulin-induced THP-1 macrophage TNF-α secretion was inhibited using a blocking antibody specific to TLR4, suggesting that TLR4 is involved in the binding of inulin to macrophages. Furthermore, we used specific kinase inhibitors to assess the involvement of inulin-induced phagocytosis and revealed that phosphoinositide 3-kinase and mitogen-activated protein kinase, especially p38, participated in phagocytosis. These results suggest that inulin affects macrophages directly by involving the TLR4 signaling pathway and stimulating phagocytosis for enhancing immunomodulation.

Volume 37, Number 6, November/December 2011, Pages 447–454 •
E-mail: yuki@mail.dendai.ac.jp

Keywords: inulin; macrophage; phagocytosis; Toll-like receptor

1. Introduction

Inulin is a polysaccharide consisting of a family of linear β-D-(2→1) polyfructofuranosyl α- D-glucoses, in which an unbranched chain of up to 100 fructose moieties is linked to a single terminal glucose [1,2]. Inulin is a widespread plant storage carbohydrate in many vegetables (chicory root, Jerusalem artichoke, onion, garlic, leek, and asparagus), cereals (wheat, rye, and barley), and fruits [3]. Polymorphically, there are several types of inulin formed, which are distinguishable by their solubility to an aqueous solution. One form of inulin, β-inulin, is instantly soluble at a temperature of 23 °C. Another form of inulin, α-inulin, is soluble at 37 °C. The third polymorphic form of inulin, γ-inulin, is insoluble in 37 °C but can be solubilized by heating up to 70–80 °C, although only in a concentrated solution (>50 mg/mL) [4].

Recent data provide evidence that inulin modulates the function of the immune system. Inulin stimulates the growth of bifidobacteria, resulting in the increased production of short-chain fatty acids and influencing the local immune effects in the gut [5]. It has also been reported that inulin activates immune cells in Peyer's patches, natural killer (NK) cells, and macrophages [5].

The mechanisms for the immune-modulating effect of inulin occur in part because inulin activates the alternative complement pathway. In particular, γ-inulin and some of the effects of α-inulin and β-inulin enhance C3 production and promote both Th1 and Th2 immune responses [6]. Inulin induces C3 deposition onto the surface of macrophages, indicating

*Address for correspondence: Yukitoshi Nagahara, Ph.D., Department of Biotechnology, College of Science and Engineering, Tokyo Denki University, Hatoyama, Hiki-gun, Saitama 350-0394, Japan. Tel.: +81-49-296-5949; Fax: +81-49-296-5162; E-mail: yuki@mail.dendai.ac.jp.

Received 25 April 2011; accepted 30 July 2011
DOI: 10.1002/biof.186
Published online 28 October 2011 in Wiley Online Library (wileyonlinelibrary.com)

that inulin-mediated immunomodulation is greatly related to macrophages. Macrophages play important regulatory and effector roles in the adaptive and innate immune systems [7]. Besides presenting antigens, macrophages produce various cytokines, such as tumor necrosis factor-α (TNF-α) and interleukin-1β, or chemokines to indirectly and directly immunomodulate phagocytosis. Macrophages phagocytose to eliminate waste and debris and to kill invading pathogens, and macrophages thus play a major role in host defense against infections, internal inflammation, and cancer progression. Recently, Toll-like receptors (TLRs) were identified as important membrane receptors on macrophages that recognize a wide range of microbial pathogens and pathogen-related products [8]. For example, TLR4 binds lipopolysaccharide (LPS) with the interaction of CD14 to facilitate recognition and enhance the phagocytosis of Gram-negative bacilli [9]. Moreover, TLR2 recognizes β-glucan by contributing the β-glucan receptor dectin-1, which activates macrophages [10].

As many polysaccharides involve TLRs to activate macrophages and enhance phagocytosis, it is possible that inulin directly stimulates macrophage phagocytosis in addition to activate alternative complement pathways. Therefore, inulin may contribute not only to eliminate pathogens but also to scavenge unwanted endogenous cells to maintain homeostasis.

In this study, we investigated whether inulin augments macrophage phagocytosis *in vitro* by using polystyrene beads and various conditions (normal or dead) of cells. Since the number of primary macrophages available for functional studies is limited due to insufficient proliferation, we mainly used the THP-1 monocytic leukemia cell line for this study. After treatment with phorbol esters, THP-1 cells differentiate into macrophage-like cells that more closely mimic native monocyte-derived macrophages than other myeloid cell lines such as U937 and HL-60 [11,12]. We also revealed the inulin recognition mechanism and phagocyte signal transduction in THP-1 macrophages.

2. Materials and methods

2.1. Cells

Resident peritoneal macrophages were harvested without stimulation from 6- to 7-week-old male mice of C3H/HeN and C3H/HeJ strains. The human monocyte leukemia THP-1 was provided by Dr. Y. Kobayashi of Toho University (Chiba, Japan). The human T cell lymphoma Jurkat was provided by Dr. T. Miyashita of Kitasato University (Kanagawa, Japan).

2.2. Reagents

Inulin was purchased from Wako (Osaka, Japan) or Sigma (St. Louis, MO) and dissolved in 100 °C water in 100 mg/mL stock solution, which includes all types of inulin (α-, β-, and γ-inulin). 5(6)-Carboxytetramethylrhodamine (TAMRA) was purchased from Invitrogen (Carlsbad, CA). Anti-TLR4 antibody and FITC-labeled anti-CD14 antibody were purchased from BioLegend (San Diego, CA) and Beckton Dickinson (Franklin Lakes, NJ), respectively.

2.3. Preparation of cells

The cells were cultured in RPMI-1640 medium supplemented with 10% fetal bovine serum (FBS) and 75 mg/L kanamycin sulfate and maintained at 37 °C in a humidified chamber under an atmosphere of 95% air and 5% CO_2. For preparation of differentiated THP-1 macrophages, THP-1 cells were incubated in a culture plate with 10% FBS-RPMI1640 including 160 nM PMA for 72 h. At the end of the incubation, the cells were washed with PBS for three times to exclude undifferentiated THP-1 cells, and medium without FBS was used throughout this study.

2.4. Phagocytosis assay

For preparation of phagocytosed normal cells, Jurkat cells were labeled with a cellular membrane-permeable dye, calcein AM. For preparation of phagocytosed apoptotic cells, Jurkat cells were treated with 6 μM sphingosine for 4 h and the cells were labeled with calcein AM. For preparation of phagocytosed necrotic cells, Jurkat cells were treated with 100 μM *N*-methyl-*N'*-nitro-*N*-nitrosoguanidine for 5 h, and the cells were labeled with cellular membrane-impermeable dye, propidium iodide (PI) [13]. C3H mice peritoneal macrophages or THP-1 macrophages (2×10^5) were incubated in 24-well plates with or without inulin at 37 °C for the indicated times. Three hours before the incubation time ended, either 6-μm or 10-μm violet dye-prestained polystyrene beads (Polysciences, Warrington, PA), normal Jurkat cells, necrotic Jurkat cells, or apoptotic Jurkat cells were added and incubated further for 3 h. After incubation, the number of engulfed beads or cells within macrophages was counted by fluorescent microscopy or phase contrast microscopy, and the macrophage phagocytic index (engulfed beads or cells number per 100 macrophages) was measured.

2.5. ELISA assay

Cells (2×10^5) were incubated with or without inulin. Culture supernatants were taken, and the concentration of TNF-α was determined by a sandwich ELISA kit (Thermo Fisher Scientific, Waltham, MA), according to the manufacturers' protocol. In brief, culture supernatants were added to an anti-TNF-α antibody-precoated 96-well plate. After incubation at r.t. for 1 h, the wells were washed and biotinylated anti-TNF-α antibody reagent was added and incubated at r.t. for 1 h. After washing, streptavidin-horseradish peroxidase and 3,3',5,5'-tetramethylbenzidine substrate solution were added, and the reaction was stopped by adding stop solution. The concentration of TNF-α was detected by using a microplate reader (MTP-32; Corona Electric, Hitachinaka, Japan) measuring the absorbance at 450 nm.

2.6. Flow cytometry analysis

Jurkat cells were treated with 250 μM 5-fluorouracil for 24 h (for preparation of apoptotic cells) or without treatment (for

preparation of normal cells), and the cells were labeled with TAMRA. For preparation of necrotic cells, Jurkat cells were treated with 100 μM *N*-methyl-*N*′-nitro-*N*-nitrosoguanidine for 5 h, and the cells were labeled with PI. THP-1 macrophages (2×10^5) were incubated in 24-well plates with or without inulin at 37 °C for 3 h. Thereafter, either normal Jurkat cells, necrotic Jurkat cells, or apoptotic Jurkat cells were added, respectively, and incubated further for 3 h. After incubation, THP-1 macrophages were collected and stained with FITC-labeled anti-CD14 antibody for 1 h. The number of engulfed cells within macrophages was measured by flow cytometer (FACS Calibur; Beckton Dickinson).

2.7. Statistical analysis

All statistical analyses were performed using Student's *t*-test. Significance was established at the $P < 0.05$ level.

3. Results

3.1. Inulin-augmented polystyrene beads phagocytosis

Generally, polysaccharide-mediated immunostimulation affects leukocytes, mainly T and B cells, NK cells, and macrophages [6,14,15]. First, we investigated the maximum dose of inulin without affecting any injury effect to macrophages. In this study, we used an *in vitro* macrophage model. When THP-1 cells were treated with 160 nM PMA for 72 h, the cells developed a macrophage-like shape and became adherent to plastic dishes [16]. These macrophage-like differentiated cells (THP-1 macrophages) were used throughout this study. Either THP-1 or THP-1 macrophages were treated with inulin, and WST-8 assay was performed to estimate cell damage (by determination of cellular NADH level). We revealed that inulin dose of up to 10 mg/mL for 24 h did not inhibit the viability of THP-1 nor THP-1 macrophages at all compared to the nonadditive control (data not shown). Moreover, 24-h treatment of 10 mg/mL inulin did not induce DNA fragmentation, which is a hallmark of apoptosis, suggesting that under 10 mg/mL doses of inulin has no cytotoxic effect to THP-1 and THP-1 macrophages (data not shown).

Therefore, we next investigated if under 10 mg/mL dose of inulin could directly activate macrophage function to stimulate the immune response. We used serum-deprived medium in further engulfment studies to rule out the effect of complements, growth factors, and cytokines. For assaying engulfment, 10-μm-diameter (the same particle size as the Jurkat cells) violet dye prestained polystyrene beads were used. After THP-1 macrophages were treated with inulin for 3 h in FBS-deprived medium, polystyrene beads were added and incubated for an additional 3 h. The number of phagocytosed beads was then counted by phase contrast microscopy observation (Fig. 1a). As shown in Fig. 1b, inulin treatment significantly increased the phagocytosis of polystyrene beads in the THP-1 macrophages, suggesting that inulin activated macrophages and resulted in an increase of phagocytosis. Inulin treatment at a dose of 1 mg/mL for 6 h doubled

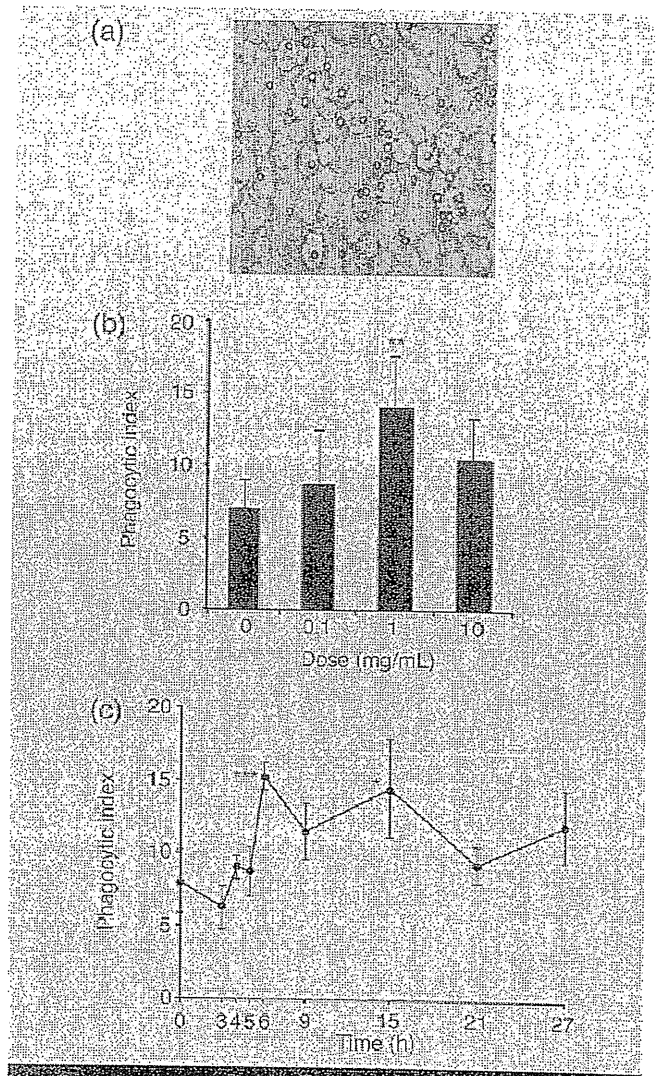

Fig. 1. Inulin-augmented phagocytosis of THP-1 macrophages. (a) Phase contrast microscopy figure of THP-1 macrophages phagocytosed 10-μm-diameter violet-colored polystyrene beads. (b) THP-1 macrophages were incubated with the indicated doses of inulin for 3 h. Thereafter, 10-μm-diameter violet-colored polystyrene beads were added and incubated further for 3 h. The number of phagocytosed beads in 100 THP-1 macrophages (phagocytic index) was counted by using phase contrast microscopy. Each bar denotes the standard deviation ($n = 6$). $^{**}P < 0.01$ compared to the nonadditive control (0 mg/mL) groups. (c) THP-1 macrophages were incubated with 1 mg/mL inulin for the indicated times. Three hours prior to the indicated times, 10-μm-diameter polystyrene beads were added and incubated further for 3 h. The number of phagocytosed beads in 100 THP-1 macrophages (phagocytic index) was counted by using phase contrast microscopy. Each bar denotes the standard deviation ($n = 4$). $^{*}P < 0.05$, $^{***}P < 0.001$ compared to nonadditive control (0 h) groups.

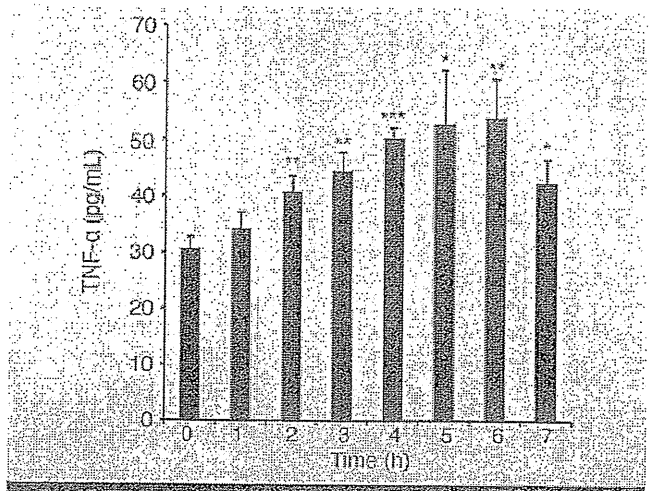

Fig. 2. Inulin treatment augmented TNF-α release from THP-1 macrophage. THP-1 macrophages were incubated with 4 mg/mL inulin for the indicated times. The released concentration of TNF-α in the culture supernatant was determined by ELISA assay, as shown in "Materials and Methods." Each bar denotes the standard deviation ($n = 3$). *$P < 0.05$, **$P < 0.01$, ***$P < 0.001$ compared to nonadditive control groups.

beads engulfment compared to the nonadditive control (basal level; Fig. 1b). Moreover, 1 mg/mL inulin treatment gradually augmented phagocytosis in a time-dependent manner, reaching a steady state in treatment of < 6 h (Fig. 1c). When using polystyrene beads smaller than 10-μm diameter (6-μm diameter) for phagocytosis assay, the basal number of polystyrene beads phagocytosed by THP-1 macrophages was significantly increased besides affecting inulin, due to the small particle size so that THP-1 macrophages were easy to phagocyte. However, phagocytosed rate (the number of beads engulfed by inulin-treated macrophages/ the number of beads engulfed by control macrophages without added inulin) was nearly identical between both particle size beads (data not shown). Therefore, we used 6-μm polystyrene beads for easy and accurate observation from the following study.

Upon activation, macrophages secrete various cytokines. We examined cytokine production of inulin to THP-1 macrophages. Macrophages secrete TNF-α upon activation. Figure 2 shows the secretion amount of TNF-α in the medium. Inulin treatment increased the secretion of TNF-α in a time-dependent manner.

3.2. Inulin-augmented phagocytosis involved TLR4

We observed inulin-augmented phagocytosis within primary macrophages. Resident peritoneal macrophages were obtained from C3H/HeN and C3H/HeJ mice. As shown in Fig. 3a, peritoneal macrophages from C3H/HeN significantly phagocytosed the polystyrene beads in response to inulin treatment. However, peritoneal macrophages from C3H/HeJ did not increase engulfment of polystyrene beads even in the presence of inulin. C3H/HeJ mice have a mutation in TLR4 but C3H/HeN mice do not [17], suggesting that inulin-augmented phagocytosis involves TLR4. To examine this hypothesis, THP-1 macrophages were treated with the anti-TLR4 antibody before inulin treatment to block TLR4. As shown in Fig. 3b, anti-TLR4 antibody treatment inhibited inulin-induced THP-1 macrophages TNF-α secretion, suggesting that inulin interacts with TLR4.

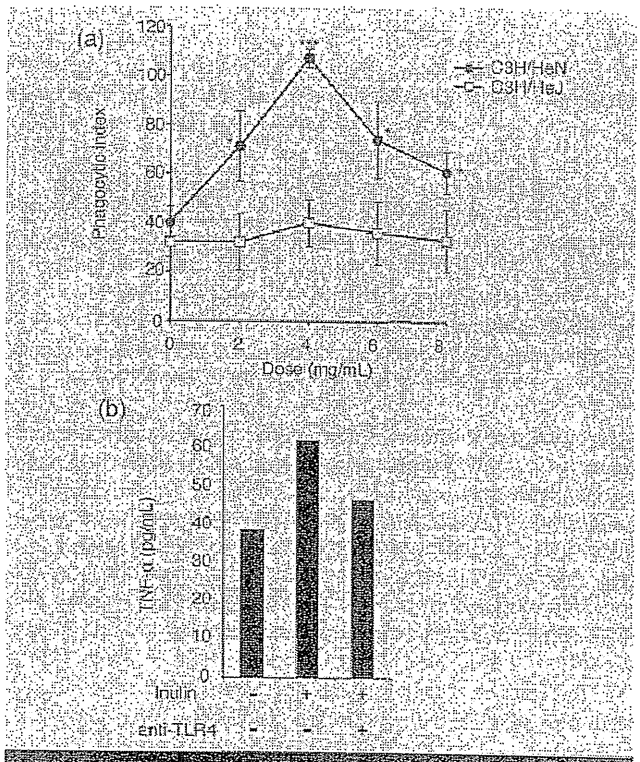

Fig. 3. Inulin augmentation of phagocytosis is related to TLR4. (a) Resident peritoneal macrophages from C3H/HeN and C3H/HeJ mice were incubated with the indicated doses of inulin for 3 h. Thereafter, 6-μm-diameter violet-colored polystyrene beads were added and incubated further for 3 h. The number of phagocytosed beads in the 100 THP-1 macrophages (phagocytic index) was counted by using phase contrast microscopy. Each bar denotes the standard deviation ($n = 3$). *$P < 0.05$, ***$P < 0.001$ compared to the nonadditive control groups. (b) THP-1 macrophages were preincubated with 10 μg/mL anti-TLR4 antibody for 1 h, and thereafter 1 mg/mL inulin was treated and incubated for 4 h. The released concentration of TNF-α in the culture supernatant was determined by ELISA assay, as shown in "Materials and Methods." Data are representative of three independent experiments.

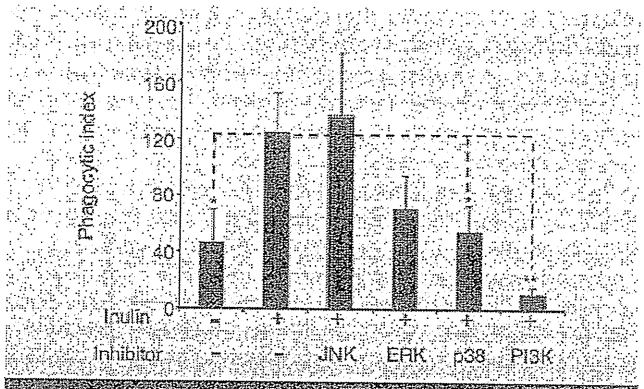

Fig. 4. Inulin-augmented phagocytosis is attenuated by MAPK and PI3K inhibitors. THP-1 macrophages were preincubated with various kinase inhibitors: 10 μM SB203580 (p38 inhibitor), 20 μM PD98059 (ERK inhibitor), 25 μM SP600125 (JNK inhibitor), and 10 μM LY294002 (PI3K inhibitor) for 1 h, and thereafter the THP-1 macrophages were incubated with 4 mg/mL inulin for 7 h. Three hours prior to the indicated times, 6-μm-diameter violet-colored polystyrene beads were added and incubated for 3 h. The number of phagocytosed beads in the 100 THP-1 macrophages (phagocytic index) was counted using phase contrast microscopy. Each bar denotes the standard deviation ($n = 3$). $^{*}P < 0.05$, $^{**}P < 0.01$ compared to inulin treatment groups.

Treatment of the Jurkat cells with 6 μM sphingosine for 4 h to Jurkat led to exposure of phosphatidylserine on their surface and DNA fragmentation, which resembled apoptosis (data not shown). Moreover, treatment with cellular membrane-impermeable dye, PI, did not stain the cells, indicating that these cells possess cellular membrane integrity (data not shown). In contrast, the Jurkat cells that were treated with 100 μM *N*-methyl-*N'*-nitro-*N*-nitrosoguanidine (a necrosis inducer) for 5 h were stained with PI [13], and the cellular membrane collapsed as a result of necrosis (data not shown).

Therefore, we labeled normal Jurkat cells and apoptotic Jurkat cells with cellular membrane-permeable dye, calcein AM, and necrotic cells stained with PI, and after incubation with THP-1 macrophages, the phagocytosed cells were counted. As shown in Fig. 5, the THP-1 macrophages phagocytosed especially the apoptotic cells. However, phagocytic index (phagocytosed cells within 100 macrophages) of Fig. 5 is relatively low and scattered (especially engulfing necrotic and apoptotic cells as objects), compared to the results engulfing 6-μm-diameter polystyrene beads. This result may occur mainly because the size of phagocytosed Jurkat cells was big that it was not easy for macrophages to phagocyte (similar low phagocyte index was obtained in Fig. 1, which used 10-μm-diameter polystyrene beads), and cell surface of phagocytosed Jurkat cells might not be in identical condition by the treatment of apoptotic or necrotic inducer. Therefore, we conducted flow cytometric phagocytosis assay to analyze

3.3. Inulin-augmented phagocytosis is attenuated by MAPK and PI3K inhibitors

We then examined the involvement of PI3K and MAPKs in inulin-augmented polystyrene beads phagocytosis. The macrophages were treated with phosphoinositide 3-kinase (PI3K) inhibitor LY294002 and mitogen-activated protein kinases (MAPKs) inhibitor (p38 inhibitor SB203580, ERK inhibitor PD98059, and JNK inhibitor SP600125), respectively, before inulin treatment. Prior to the treatment, we have checked that all the inhibitors were not toxic at the dose and time used in this study (data not shown). Among these inhibitor treatments, the PI3K and p38 inhibitors significantly blocked the phagocytosis of beads compared to the inulin-treatment groups (Fig. 4). The ERK inhibitor also suppressed phagocytosis, whereas the JNK inhibitor had no effect on phagocytosis.

3.4 Inulin treatment strongly augmented the phagocytosis of apoptotic cells

After examining the effect of inulin on augmentation of phagocytosis using beads, we next used a more physiological model, cancer cells. To investigate the relationship between THP-1 macrophages and phagocytosis, we used normal, apoptotic, and necrotic human T cell lymphoma Jurkat cells to engulf the model cells, in order to investigate the relationship between THP-1 macrophages and phagocytosis.

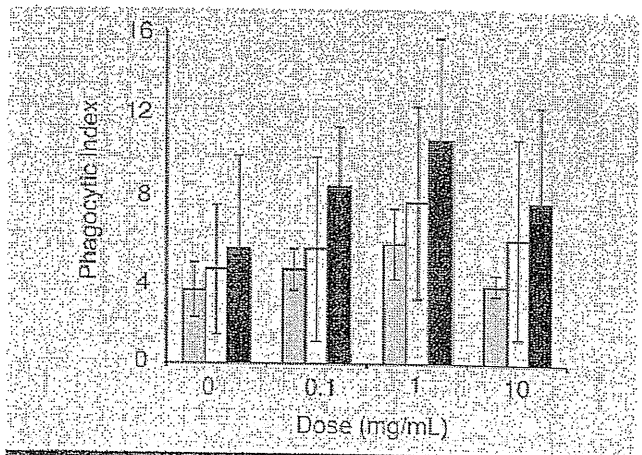

Fig. 5. Inulin treatment augmented phagocytosis of apoptotic cell to THP-1 macrophage. THP-1 macrophages were incubated with the indicated doses of inulin for 3 h. Thereafter, either fluorescent dye labeled normal (gray bar), necrosis- (white bar), or apoptosis- (black bar) induced Jurkat cells were added, respectively, and incubated further for 3 h. The number of phagocytosed cells in the 100 THP-1 macrophages (phagocytic index) was counted by using fluorescent microscopy. Each bar denotes the standard deviation ($n = 4$).

large number of macrophages (10,000 cell counts) compared to microscopic assay (100 cell counts), so as to estimate the phagocytosis rate precisely.

We used a red fluorescent dye, TAMRA, to label normal Jurkat cells and apoptotic Jurkat cells, or PI to label necrotic Jurkat cells. In this assay, we treated another apoptosis inducer, 5-fluorouracil, which similarly induces apoptosis as sphingosine. After incubation with THP-1 macrophages, macrophages were labeled with FITC-anti-CD14 antibody. Using flow cytometry, Jurkat cells-phagocytosed THP-1 macrophage cells can be detected in red- and green-fluorescence double positive area (Fig. 6a). In contrast, nonphagocytosed Jurkat cells are able to observe in red-fluorescence single positive area. As shown in dot plot of Fig. 6a, THP-1 macrophages, which engulfed apoptotic Jurkat cells by inulin, can be clearly determined.

This flow cytometric analysis was performed with engulfing normal, necrotic, and apoptotic Jurkat cells to THP-1 macrophages, and the percentage of Jurkat cell-phagocytosed THP-1 cells was analyzed. As shown in Figs. 6b–6d, THP-1 macrophages slightly increased engulfment of normal and necrotic cells by inulin, whereas significant uptake was observed in phagocytosing apoptotic cells. Moreover, inulin-augmented apoptotic cells phagocytosis was blocked by MAPK inhibitors and PI3K inhibitor (Fig. 6d) or affecting anti-TLR4 antibody (Fig. 6e).

4. Discussion

In this study, we demonstrated that inulin induced the progression of phagocytosis in THP-1 macrophages in a time- and dose-dependent manner. Doses around 1 mg/mL had maximal effect, and significant progression of phagocytosis occurred at over 6 h. Inulin-augmented phagocytosis occurred not only in polystyrene beads but also in apoptotic cells. This inulin-induced phagocytosis seemed to be dependent on TLR4. Moreover, inulin-induced phagocytosis was regulated by the PI3K and MAPK signaling pathways.

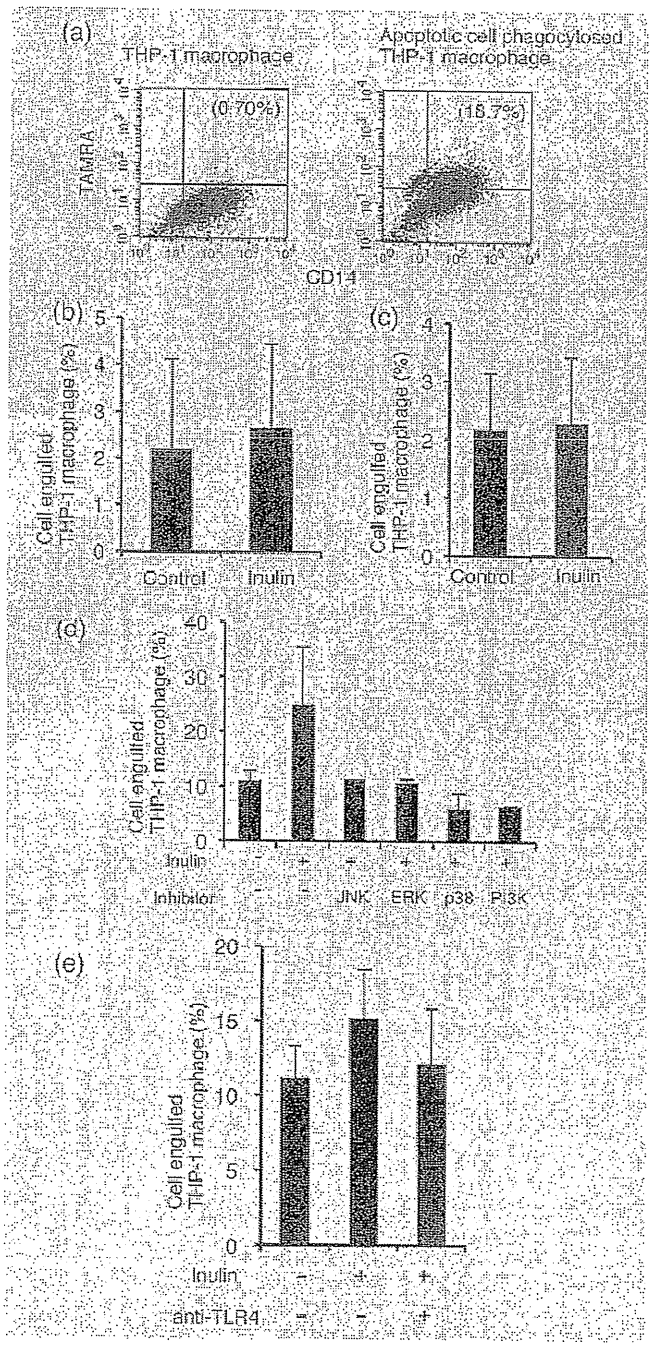

Fig. 6. Inulin-augmented phagocytosis of apoptotic cells is related to PI3K and TLR4. THP-1 macrophages were preincubated with or without various kinase inhibitors: 10 μM SB203580, 20 μM PD98059, 25 μM SP600125, and 10 μM LY294002 or 10 μg/mL anti-TLR4 antibody for 1 h, and thereafter the THP-1 macrophages were incubated with 4 mg/mL inulin for 7 h. Three hours prior to the indicated times, either normal, necrosis-, or apoptosis-induced fluorescent labeled Jurkat cells were added and incubated for 3 h. The percentage of phagocytosed Jurkat cells was analyzed by flow cytometry. (a) Dot plot flow cytometric analysis data of Jurkat cell engulfed THP-1 macrophages. Values in parenthesis resemble the percentages of TAMRA and CD14 double positive region (Jurkat cell engulfed THP-1 macrophage) of total cells. Data are representative of four independent experiments. (b) Determination of inulin effect to THP-1 macrophage engulfing normal cells. Each bar denotes the standard deviation ($n = 2$). (c) Determination of inulin effect to THP-1 macrophage engulfing necrotic cells. Each bar denotes the standard deviation ($n = 2$). (d) Determination of inulin effect to THP-1 macrophage engulfing apoptotic cells and the effect to MAPK inhibitors and PI3K inhibitor. Each bar denotes the standard deviation ($n = 2$). (e) Effect of anti-TLR4 antibody. Each bar denotes the standard deviation ($n = 2$).

It has been reported that inulin is a potent activator of the alternative complement pathway. Inulin induced C3 deposition onto the surface of macrophages resulting in an activation of adaptive immunity by promoting Th1 and Th2 and innate immunity by opsonization phagocytosis of macrophages *in vivo* [6]. However, the precise mechanism of the inulin-induced adjuvant effect is not clear. On the other hand, recent studies reported that oligosaccharides might affect immune cells such as NK cells, macrophages, T cells, and B cells *in vitro* [18,19]. In this study, we used serum-free medium in the experiment to exclude the effect of complement and cytokines. Inulin augmented phagocytosis in the serum-free condition, suggesting that inulin directly affected the macrophages. As expected, the addition of fresh serum upregulated inulin-induced phagocytosis and TNF-α production (data not shown).

TLRs are a family of receptors for the recognition of bacteria and play an important role in innate immunity [8]. Ligands for TLRs vary with each TLR. They respond to various components of bacteria such as cell wall components, bacterial DNA, RNA, and flagella [20–22]. For example, TLR2 binds to β-glucan and TLR4 binds to LPS [20]. Recent data indicated that TLR4 also binds to other polysaccharides such as mannan [23], safflower polysaccharides [24], and inulin structure-like polysaccharide [25], and it is presumed that TLR4 binds to various oligosaccharides. In this study, we revealed from using mutant TLR4 mice and blocking antibody experiments that inulin seems to contact TLR4 to activate macrophages and trigger phagocytosis. However, the precise manner in which inulin binds to TLR4 (specifically whether other components are required) needs to be clarified.

Ligand-bound TLR4 activates the PI3K and MAPK downstream kinase pathways and induces proinflammatory cytokine gene expression [26]. We therefore used PI3K and MAPK inhibitors to estimate the effect of PI3K and MAPK in inulin-mediated phagocytosis. In this study, PI3K and one of the MAPK, p38, were involved in the inulin-mediated phagocytosis. Similar results showing that phagocytosis by macrophage is involved in Akt activation, which is a downstream kinase of PI3K, were obtained earlier [27]. Since the activation of Akt promotes cell survival, the uptake of a foreign body may prompt the enhancement of macrophage survival during phagocytosis digestion. Moreover, it has been reported that PI3K signaling is involved in the activation of the Rho family GTPases, leading to the initiation of actin polymerization for phagocytosis [28]. In addition, p38 is involved in encapsulating foreign bodies during phagocytosis in *Drosophila* [29]. Similarly, inhibition of p38-inhibited phagocytosis, presumably due to encapsulate failure, was demonstrated in this study.

We have revealed that inulin especially augmented the uptake of apoptotic cells. Apoptotic cells expose numerous apoptosis-specific cell surface ligands during apoptosis, such as phosphatidylserine, to bind existing phagocytic receptors in macrophages. However, the other cells used in this study (normal cells and necrotic cells) have little ligands to bind macrophages. Therefore, the apoptotic cells, rather than the other cells (normal and necrotic cells), tended to undergo phagocytosis. Based on this evidence, inulin treatment to macrophages seemed to activate nonspecific phagocytosis by PI3K and p38 activation, rather than specific upregulation of the phagocytic receptors.

In this study, inulin doses around 1 mg/mL were needed to activate macrophages. Cotlove et al. reported that an intravenous injection of 75 mg/kg of inulin to cow resulted in a level of 0.6 mg/mL inulin in serum [30]. Given this result, a blood concentration of inulin of about 1 mg/mL may occur despite the fact that inulin disappears quickly from the blood.

Overall, inulin augmented phagocytosis, especially in apoptotic cells. The activation of innate immunology by inulin may be a promising agent for immunomodulation and for anticancer therapy.

Acknowledgement

The authors are thankful to Ms. Kayo Motomura for technical assistance.

References

[1] Jenkins, D. J., Kendall, C. W., and Vuksan, V. (1999) Inulin, oligofructose and intestinal function. J. Nutr. 129, 1431S–1433S.
[2] Silva, D. G., Cooper, P. D., and Petrovsky, N. (2004) Inulin-derived adjuvants efficiently promote both Th1 and Th2 immune responses. Immunol. Cell Biol. 82, 611–616.
[3] van Loo, J., Coussement, P., de Leenheer, L., Hoebregs, H., and Smits, G. (1995) On the presence of inulin and oligofructose as natural ingredients in the western diet. Crit. Rev. Food Sci. Nutr. 35, 525–552.
[4] Cooper, P. D. and Carter, M. (1986) Anti-complementary action of polymorphic "solubility forms" of particulate inulin. Mol. Immunol. 23, 895–901.
[5] Watzl, B., Girrbach, S., and Roller, M. (2005) Inulin, oligofructose and immunomodulation. Br. J. Nutr. 93 Suppl 1, S49–S55.
[6] Kerekes, K., Cooper, P. D., Prechl, J., Jozsi, M., Bajtay, Z., and Erdei, A. (2001) Adjuvant effect of gamma-inulin is mediated by C3 fragments deposited on antigen-presenting cells. J. Leukoc. Biol. 69, 69–74.
[7] Dale, D. C., Boxer, L., and Liles, W. C. (2008) The phagocytes: neutrophils and monocytes. Blood 112, 935–945.
[8] Uematsu, S. and Akira, S. (2007) Toll-like receptors and Type I interferons. J. Biol. Chem. 282, 15319–15323.
[9] Chow, J. C., Young, D. W., Golenbock, D. T., Christ, W. J., and Gusovsky, F. (1999) Toll-like receptor-4 mediates lipopolysaccharide-induced signal transduction. J. Biol. Chem. 274, 10689–10692.
[10] Brown, G. D., Herre, J., Williams, D. L., Willment, J. A., Marshall, A. S., and Gordon, S. (2003) Dectin-1 mediates the biological effects of beta-glucans. J. Exp. Med. 197, 1119–1124.
[11] Auwerx, J. (1991) The human leukemia cell line, THP-1: a multifaceted model for the study of monocyte-macrophage differentiation. Experientia 47, 22–31.
[12] Maess, M. B., Sendelbach, S., and Lorkowski, S. (2010) Selection of reliable reference genes during THP-1 monocyte differentiation into macrophages. BMC Mol. Biol. 11, 90.
[13] Ha, H. C. and Snyder, S. H. (1999) Poly(ADP-ribose) polymerase is a mediator of necrotic cell death by ATP depletion. Proc. Natl. Acad. Sci. USA 96, 13978–13982.
[14] Han, S. B., Park, S. H., Lee, K. H., Lee, C. W., Lee, S. H., Kim, H. C., Kim, Y. S., Lee, H. S., and Kim, H. M. (2001) Polysaccharide isolated from the radix of Platycodon grandiflorum selectively activates B cells and macrophages but not T cells. Int. Immunopharmacol. 1, 1969–1978.

[15] Kim, G. Y., Lee, J. Y., Lee, J. O., Ryu, C. H., Choi, B. T., Jeong, Y. K., Lee, K. W., Jeong, S. C., and Choi, Y. H. (2006) Partial characterization and immunostimulatory effect of a novel polysaccharide-protein complex extracted from *Phellinus linteus*. Biosci. Biotechnol. Biochem. 70, 1218–1226.

[16] Kurosaka, K., Watanabe, N., and Kobayashi, Y. (1998) Production of proinflammatory cytokines by phorbol myristate acetate-treated THP-1 cells and monocyte-derived macrophages after phagocytosis of apoptotic CTLL-2 cells. J. Immunol. 161, 6245–6249.

[17] Poltorak, A., He, X., Smirnova, I., Liu, M. Y., Van Huffel, C., Du, X., Birdwell, D., Alejos, E., Silva, M., Galanos, C., Freudenberg, M., Ricciardi-Castagnoli, P., Layton, B., and Beutler, B. (1998) Defective LPS signaling in C3H/HeJ and C57BL/10ScCr mice: mutations in Tlr4 gene. Science 282, 2085–2088.

[18] Murosaki, S., Muroyama, K., Yamamoto, Y., Kusaka, H., Liu, T., and Yoshikai, Y. (1999) Immunopotentiating activity of nigerooligosaccharides for the T helper 1-like immune response in mice. Biosci. Biotechnol. Biochem. 63, 373–378.

[19] Du, Z., Kelly, E., Mecklenbrauker, I., Agle, L., Herrero, C., Paik, P., and Ivashkiv, L. B. (2006) Selective regulation of IL-10 signaling and function by zymosan. J. Immunol. 176, 4785–4792.

[20] Takeuchi, O. and Akira, S. (2001) Toll-like receptors; their physiological role and signal transduction system. Int. Immunopharmacol. 1, 625–635.

[21] Mizel, S. B. and Snipes, J. A. (2002) Gram-negative flagellin-induced self-tolerance is associated with a block in interleukin-1 receptor-associated kinase release from toll-like receptor 5. J. Biol. Chem. 277, 22414–22420.

[22] Krieg, A. M. and Vollmer, J. (2007) Toll-like receptors 7, 8, and 9: linking innate immunity to autoimmunity. Immunol. Rev. 220, 251–269.

[23] Figueiredo, R. T., Fernandez, P. L., Dutra, F. F., Gonzalez, Y., Lopes, L. C., Bilitencourt, V. C., Sassaki, G. L., Barreto-Bergter, E., and Bozza, M. T. (2010) TLR4 recognizes *Pseudallescheria boydii* conidia and purified rhamnomannans. J. Biol. Chem. 285, 40714–40723.

[24] Ando, I., Tsukumo, Y., Wakabayashi, T., Akashi, S., Miyake, K., Kataoka, T., and Nagai, K. (2002) Safflower polysaccharides activate the transcription factor NF-kappa B via Toll-like receptor 4 and induce cytokine production by macrophages. Int. Immunopharmacol. 2, 1155–1162.

[25] Yoon, Y. D., Han, S. B., Kang, J. S., Lee, C. W., Park, S. K., Lee, H. S., and Kim, H. M. (2003) Toll-like receptor 4-dependent activation of macrophages by polysaccharide isolated from the radix of Platycodon grandiflorum. Int. Immunopharmacol. 3, 1873–1882.

[26] Li, X., Jiang, S., and Tapping, R. I. (2010) Toll-like receptor signaling in cell proliferation and survival. Cytokine 49, 1–9.

[27] Reddy, S. M., Hsiao, K. H., Abernethy, V. E., Fan, H., Longacre, A., Lieberthal, W., Rauch, J., Koh, J. S., and Levine, J. S. (2002) Phagocytosis of apoptotic cells by macrophages induces novel signaling events leading to cytokine-independent survival and inhibition of proliferation: activation of Akt and inhibition of extracellular signal-regulated kinases 1 and 2. J. Immunol. 169, 702–713.

[28] Han, J., Luby-Phelps, K., Das, B., Shu, X., Xia, Y., Mosteller, R. D., Krishna, U. M., Falck, J. R., White, M. A., and Broek, D. (1998) Role of substrates and products of PI 3-kinase in regulating activation of Rac-related guanosine triphosphatases by Vav. Science 279, 558–560.

[29] Shinzawa, N., Nelson, B., Aonuma, H., Okado, K., Fukumoto, S., Miura, M., and Kanuka, H. (2009) p38 MAPK-dependent phagocytic encapsulation confers infection tolerance in Drosophila. Cell Host Microbe 6, 244–252.

[30] Cotlove, E. (1961) Simple tail vein infusion method for renal clearance measurements in the rat. J. Appl. Physiol. 16, 764–766.